Graphical abstract

Numerical simulations of rear point contacted solar cells on 2.2 Ωcm p-type c-Si substrates

Juan M. López-González, I. Martín*, P. Ortega, A. Orpella and R. Alcubilla

* e-mail: <u>isidro.martin@upc.edu</u>

In this work, we highlight the importance of a 3D accurate modelling of rear point-contact p-type c-Si solar cells particularly when the c-Si substrates are not highly-doped, like the 2.2 Ωcm c-Si ones used in this work as experimental reference. For such relatively low-doped substrates, the simpler and widely-used 1D approach leads to important deviations in V_{oc} an *FF* that significantly impacts on the optimum rear pitch predicted by the simulations.

Numerical simulations of rear point contacted solar cells on 2.2 Ωcm p-type c-Si substrates

Juan M. López-González, I. Martín*, P. Ortega, A. Orpella and R. Alcubilla

Departament d'Enginyeria Electrònica, Universitat Politècnica de Catalunya ,

C/ Jordi Girona 1-3, Mòdul C4, 08034 Barcelona, Spain

e-mail: isidro.martin@upc.edu

Rear surface of high-efficiency crystalline silicon (c-Si) solar cells is based on a combination of dielectric passivation and point-like contacts. In this work we develop a 3D model for these devices based on 2.2 Ωcm p-type c-Si substrates. We validate the model by comparison to experimental results allowing us to determine an optimum design for the rear pattern. Additionally, the 3D model results are compared to the ones deduced from a simpler and widely-used 1D model. While the maximum efficiency predicted by both models is approximately the same, large deviations are observed in open circuit voltage (V_{oc}) and fill factor (*FF*). 1D simulations overestimate V_{oc} since Dember and electrochemical potential

drops are not taken into account. On the contrary, *FF* is underestimated due to higher ohmic losses along the base when 1D analytical model is used. These deviations are larger for relatively low-doped substrates, as the ones used in the experimental samples reported hereby, and poor passivated contacts. As a result, 1D models could mislead to too short optimum rear contact spacing.

1. Introduction

In order to make photovoltaic energy competitive, the main objective of the photovoltaic industry for terrestrial applications is the reduction of the fabrication costs. For solar cells based on crystalline silicon (c-Si), two main trends have been identified during the last years: the reduction of the wafer thickness and the increase in energy conversion efficiency [1]. In this case, carrier recombination at front and rear surfaces has become of paramount relevance in the device performance. In typical industrial devices the rear surface traditionally consisted of an Al back surface field (Al-BSF). However, this technology is not well suited to this new scenario, since alloyed Al-BSF does not provide enough surface passivation for the thinner devices [2]. Additionally, such thin wafers bow during thermal firing of the metallic pastes causing wafer cracking and reducing fabrication yield.

In the last years, different approaches based on the Passivated Emitter and Rear Cell (PERC) concept [3] have been developed in order to close the gap between laboratory scale and industrial solar cells. This type of cell combines excellent rear surface passivation provided by a dielectric layer with local point contacts. As a result, much lower effective rear surface recombination velocities ($S_{\text{eff-rear}}$) compared to Al-BSF cells are achieved. In order to create the point contact scheme in an industrial environment, laser processing has been successfully applied to perform rear contacts in p-type c-Si substrates leading to the so called laser-fired contact (LFC) technique [4]. This technique consists of a laser spot that locally fires the aluminum film (~2 μm) through a passivating dielectric layer contacting the base in a

very cost-effective way. Moreover, if proper laser conditions are used, an Al-doped p+ region can be simultaneously created providing passivation at the contacts by means of a back surface field (BSF) and ensuring good ohmic contacts independently of the wafer resistivity [5]. Recently, an interesting alternative to perform point contacts to p-type substrates has been proposed based on laser processing of Al_2O_3/SiC_x layers before metallic aluminum deposition. In those regions, the dielectric is ablated while simultaneously part of the aluminum atoms located at the film stack creates a p^+ region. In this case, effective surface recombination velocities of about $2x10^3$ cm/s have been demonstrated with specific point contact resistances below 1 $m\Omega cm^2$ [6].

Optimization of rear point contact scheme, i.e determination of the optimum point contact pitch, reflects the trade-off between rear recombination and base ohmic losses. The most common approach to this procedure is based on the reduction of the 3D effects to equivalent parameters that can be treated in a 1D approach, typically an equivalent $S_{eff-rear}$ and a base series resistance, r_{base}. Many works can be found in the literature where 1D simulations combined with analytical and/or semi-empirical models are applied to study rear locally contacted solar cells [7-12]. 2D approaches have been scarcely used because of the difficulty in the definition of a simulation domain that can be correctly extrapolated (when the unitary cell that contains rear contacts is repeated, the point-like contact is approximated by a finger-like geometry) [5,13]. Despite all these simpler approaches, the inherent 3D effects in a rear point contacted solar cell require 3D modeling to obtain accurate results as the ones reported in references [14-16]. In this case the simulation domain can be reduced to a geometrically irreducible simple domain which, by repeating it along the solar cell, reproduces the full cell structure with minimum distortion [17].

In this paper we use our experience on bipolar device modeling [18] for developing a 3D

numerical model using commercial TCAD software (Silvaco-ATLAS [19]) to be applied to PERC-type solar cells fabricated on 2.2 Ωcm FZ p-type substrates. The main feature of these cell is the application of the laser processing of Al_2O_3/SiC_x stacks to define the point-like rear contact. Details of the fabrication process are shown in reference [20]. After the description of the developed model, the paper is divided in two parts. In the first part and after comparing simulations to experimental data in order to validate the model, we determine the surface recombination velocity at the rear contacts, S_{cont}, and the specific contact resistance, $r_{c\text{-}rear}$, at the rear contacted regions for the fabricated devices. The obtained results will allow us to use simulations as a tool to diagnose efficiency losses in our fabricated devices and to determine the optimum rear pitch. In the second part, we analyze the main differences that exist between the more complex but more accurate 3D simulations and the widely-used 1D approach.

2. Description of the device model

In this section, we describe in detail certain characteristics that are unique to our model. Particularly, we explain in detail the geometry of simulation domains, the optical and the ohmic losses model. The rest of the models and parameters, that are kept constant in all the simulations and treated in a conventional way, are presented in Appendix A.

2.1. Geometric model

The simulated structure follows the geometrical features of our fabricated devices. On the front face, a metal finger width and distance between fingers of 16 and 800 μm respectively are defined. The emitter contacted area is the same area defined by the fingers. On the rear surface we create the contacts by laser processing the Al_2O_3/SiC_x film leading to round spots

with a diameter of about 50 μm (see reference [6]). For the shake of simplicity, in the model we define rear contacts with a square shape of 50 $\times$ 50 μm^2. The distance between the center of every rear contact or pitch (*p*) is varied between 200 and 1600 μm.

Since solar cell geometry is highly symmetric, the simulation domain can be reduced to a geometrically irreducible domain. The simple domain in the case of rear contact pitch of 1600 μm has an area of 400 x 800 μm^2, for 200, 400 and 800 μm the area is 400 x 400 μm^2 while for pitches of 300 and 600 μm the area is 1200 x 600 μm^2 (see Figure 1(a)). Notice that all the basic simulation domains include at least one anode (base contact) and one cathode (emitter contact) electrodes. Then, silicon solar cell performance can be obtained simulating only the basic 3D simulation domain and properly scaling the electrical current, i.e cells electrically connected in parallel, and adding the busbar contribution to the series resistance. Hence, the solar cell area is considered a periodic repetition of the basic simulation domain neglecting the differences located at the corners, edges and bus contacted regions.

2.2. Optical model

Fabricated solar cells use a textured surface with inverted pyramids and a single antireflection coating (a thermal SiO$_2$ layer 100 nm thick). In order to decrease the complexity when defining device geometry, the simulated structure considers a flat front surface with total light transmission. The reflectance losses are modeled in the following way. We experimentally determine the solar cell reflectance at a region out of the busbar, $R_{exp}(\lambda)$. The spot of this measurement include several fingers. However, the reflectance of these fingers is automatically included in the simulations in the basic domain (2% area). Thus, this reflectance must be subtracted from the experimental value. On the other hand, the busbar
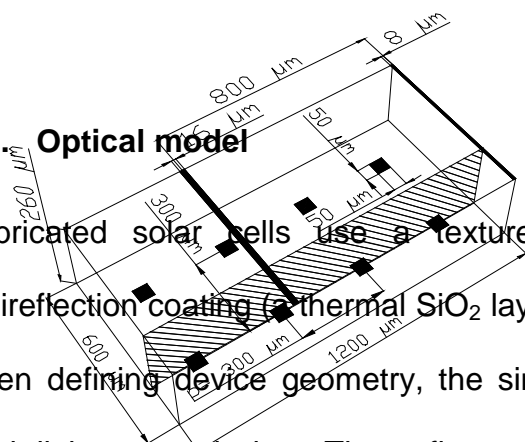
reflectance must be added (0.7% area). Then, we calculate a modified AM1.5G solar spectrum using:

$$S_{in}(\lambda) = S_{AM1.5}(\lambda)\left[1 - R(\lambda)\right] = S_{AM1.5}(\lambda)\left[1 - (R_{exp}(\lambda) - 0.02 + 0.007)\right] \qquad (1)$$

where $R(\lambda)$ is the light reflectance, $S_{AM1.5}(\lambda)$ is the standard AM1.5G spectral irradiance and $S_{in}(\lambda)$ is the modified incident solar spectral irradiance introduced into the simulations. Figure 2 shows the result of these calculations.

In order to reduce computing requirements, only one internal light bounce at the rear surface has been considered (94% back reflectance) with total transmission semiconductor-air at the front. This simplification underestimates the light absorption in the 1000-1200 nm wavelength range since in the experimental samples some light confinement is present allowing several internal reflections and thus lengthening the optical path of these photons. To reproduce this effect, silicon absorption coefficients in this range are conveniently increased so that simulated internal quantum efficiency matches the experimental one for the sample with 650 µm rear contact pitch, as shown in Figure 3. In this way, we can match the experimental short-circuit current with a negligible distortion of the photogenerated carrier profile.

2.3. Ohmic Model losses

The ohmic losses related to the front metallization include fingers, busbar as well as resistance at the emitter contact. The model considers the fingers as equipotential surfaces. Then, the easiest way to introduce them is an equivalent front contact resistance ($r_{c\text{-front}}$) in Ωcm^2 units. Notice that $r_{c\text{-front}}$ is not a lumped resistance but is distributed along the finger length. A solar cell with pitch 250 µm is used to estimate $r_{c\text{-front}}$ leading to $r_{c\text{-front}} \cong 7$ mΩcm^2

which correspond to a specific front series resistance in the final device of 0.35 Ωcm^2 (total cell area of 4 cm^2 and 2% of emitter contacted area). On the other hand, a rear contact resistance is included at the back electrode ($r_{c\text{-rear}}$). The value of this parameter is discussed in section 3.1.

3. Results and discussion

3.1. Validation of the model

Figure 4 shows the experimental photovoltaic parameters - where J_{sc}, V_{oc}, FF and η are the short circuit current density, the open circuit voltage, the fill factor and the energy conversion efficiency respectively - of solar cells fabricated following the procedure reported in reference [20] based on Al_2O_3/SiC_x laser processing. We use the model described in the previous section to reproduce the experimental results of two fabrication runs, labeled as Run A and Run B, where slightly different rear metallization steps were performed. Assuming that the rear passivated regions maintain a surface recombination velocity, S_{pas}, of 10 cm/s [20], the only free parameters of the model are the surface recombination velocity at the rear contacted areas, S_{cont}, and their contact resistance, $r_{c\text{-rear}}$. As it can be seen in Figure 4, our model precisely follows the experimental trends in both cases with S_{cont} and $r_{c\text{-rear}}$ values shown in Table I indicating a trade-off between contact passivation and contact resistance. Apart from this result, based on the high accuracy in describing the experimental trends, the simulation model is validated and, thus, it can help us to envisage the efficiency limit of our structures. In particular, Figure 5 shows the dependence of cell efficiency on rear pitch for two S_{cont} values: the one at the currently finished devices, 3.5×10^4 cm/s; and the one deduced from test samples, 2×10^3 cm/s [20], both with $r_{c\text{-rear}} = 2$ mΩcm^2. As it can be seen, there is a

strong dependence of the optimum pitch on this cell parameter changing from about 550 μm for the poor passivated contacts to about 350 μm in case of good passivation. Additionally, the S_{cont} reduction also impacts on the cell efficiency increasing it from 21.1 % to 22.0 %. We can conclude that for an optimized design the optimum pitch must evolve with the passivation of the contacts and an accurate model of the device is crucial in this task. In the next section, we underline the differences between the 3D simulations and the widely-used 1D approach for modeling rear locally contacted solar cells.

3.2. Differences between 3D and 1D models

As 1D model, we use Fischer's equation [7] in order to calculate a rear surface recombination velocity, $S_{eff\text{-}rear}$, with the same S_{pas} and S_{cont} than in the 3D model:

$$S_{eff-rear} = \frac{D}{w} \times \left[\frac{p}{2w\sqrt{\pi f_c}} \times \tan^{-1}\left(\frac{2w}{r}\right) - e^{\left(-w/p\right)} + \frac{D}{f_c w S_{cont}} \right]^{-1} + \frac{S_{pas}}{1-f_c} \qquad (2)$$

where D is the electron diffusivity (30.59 cm^2/s for 2.2 p-type Ωcm), w is the wafer thickness (260 μm), r is the contact radius (to keep the same contacted area in both 1D and 3D models, we assume circular contacts with a radius of 28 μm), and f_c is the contacted area fraction ($f_c = \pi r^2/p^2$). Then, this $S_{eff,rear}$ value is introduced in PC-1D [21] where we reproduce the main features of our devices (shadowing, phosphorus profile, front surface recombination velocity, etc.). In this case, series resistance ($r_{PC\text{-}1D}$) is modeled as a lumped element with three terms. The first one is a constant term that takes into account resistive losses at the front grid ($r_{front} = 0.35$ Ωcm^2); the second one includes the base resistance of a point-like contact scheme (r_{base}) [10]; and the third one takes into account the contact resistance at the local contacts

based on the $r_{c\text{-rear}}$ values deduced from 3D simulations ($r_{c\text{-rear}} = 2$ mΩcm^2). The final expression for $r_{PC\text{-1D}}$ is:

$$r_{PC-1D} = r_{front} + r_{base} + \frac{r_{c-rear}}{f_c} = 0.35 + \frac{\rho_B r}{2f_c} \times \tan^{-1}\left(\frac{2w}{r_c}\right) + \rho_B w\left(1 - e^{\left(-w/p\right)}\right) + \frac{r_{c-rear}}{f_c} \tag{3}$$

Figure 6 shows the 1D simulation results as a function of pitch for $S_{cont} = 5 \times 10^6$ cm/s (no passivation) and 2×10^3 cm/s together with the corresponding 3D simulations for a direct comparison. Despite maximum achievable efficiencies agree well between 1D and 3D models, a steeper decay of conversion efficiency for 1D simulations is observed for long pitches. Moreover, the optimum pitch also differs resulting in a shift to shorter values for 1D simulations. As it can be seen in Figure 6, all these deviations are mainly related to differences in V_{oc} and FF while the differences in J_{sc} are negligible.

Focusing on V_{oc}, 1D simulations overestimate this parameter in the explored range particularly for the case of $S_{cont} = 5 \times 10^6$ cm/s. Two main effects are responsible for potential drops along the p-type base: the Dember potential and the change in the electrochemical potential.

The Dember potential is related to ambipolar carrier transport. Under open-circuit conditions and illumination, charge carriers must travel through the base to reach the rear surface where the main recombination mechanism is taking place. The difference in the mobility and hence diffusivity between electrons and holes induces an electric field pointing to the rear surface, i.e. the holes move slower and the electric field helps in keeping both carrier flows equal. When it is integrated along the base, a potential drop appears. In 1D, the potential drop due to this effect, ΔV_{Dember}, for a p-type substrate can be calculated with equation (4) where all the symbols have their usual meaning and x-axis is defined as in Figure 1 with x=0 being the

edge of the space charge region at the front surface (a good explanation about this well-known effect can be found in Appendix A3 of Fischer's thesis [7]).

$$\Delta V_{Dember} = V_t \left(\frac{\mu_n - \mu_p}{\mu_n + \mu_p} \right) \ln \left(\frac{\Delta n(x=0) + \frac{\mu_p}{\mu_n + \mu_p} \cdot N_A}{\Delta n(x=w) + \frac{\mu_p}{\mu_n + \mu_p} \cdot N_A} \right) \tag{4}$$

On the other hand, the drop in the electrochemical potential is linked to the fact that the majority carrier profile is not constant along the device. At mid- and high-injection levels, the majority carrier density, $p \cong \Delta n + N_A$, is higher at x=0 than at x=w bringing hole quasi-Fermi level closer to the valence band at x=0. Thus, the electrochemical potential drop, $\Delta V_{electrochemical}$, can be expressed as follows:

$$\Delta V_{electrochemical} = V_t \cdot \ln \left(\frac{\Delta n(x=0) + N_A}{\Delta n(x=w) + N_A} \right) \tag{5}$$

As it can be deduced from equations (4) and (5), both effects vanish at low-injection levels where $\Delta n \ll N_A$ and when $\Delta n(x=0)$ equals $\Delta n(x=w)$, i.e. for well passivated contacts. Figure 7(a) shows a cross-section centered at the contacts of $\Delta n(x,y)$ for the case of $S_{cont} = 5 \times 10^6$ cm/s and p= 800 μm (notice that the basic domain is 400 μm long, i.e. half of the pitch) and considering the structure under open circuit conditions. For a direct comparison, we plot $\Delta n(x)$ from 3D simulations at y= 400 μm, the profile between emitter and base contacts, and the same magnitude calculated by PC-1D with an equivalent $S_{eff,rear}$ of 61 cm/s calculated using equation (2). At the edge of the space charge region, $\Delta n(x=0)$ is similar in both cases to about 2.0×10^{15} cm^{-3} with a small deviation related to the difference in V_{oc} used in each case. However, an important difference in Δn is found at the rear contact where 3D simulation gives

2.3x10^{12} cm^{-3} while PC-1D yields 1.9x10^{15} cm^{-3}. Notice that with such a high S_{cont} value in the real device Δn is anchored to very low values at the rear contacts and any calculation of an equivalent $S_{eff,rear}$ would yield a very distorted Δn profile.

Table II shows the Dember and electrochemical potential drops calculated using equations (4) and (5) for three S_{cont} values. Additionally, V_{oc} values calculated with 3D simulations and the equivalent 1D model are also shown. Notice that ΔV_{Dember} and $\Delta V_{electrochemical}$ explain the main differences in V_{oc} between both simulations. In addition, due to the higher Δn value along the whole base found in 1D simulations, V_{oc} is further overestimated due to mid-injection effects that account for the rest of the difference between 1D and 3D simulations. Additionally, in the last line of Table II we show the calculations for a 0.4 Ωcm p-type substrate (N_A= 3.7x10^{16} cm^{-3}). In this case, even with no passivation at the contacts the difference between 3D and 1D approach is only 1 mV since mid- or high-injection levels are not reached under open-circuit conditions at 1 sun illumination. As a summary, we can conclude that 1D approach could lead to strong deviations in V_{oc} for devices with poor passivated contacts and relatively low-doped substrates, as the ones used in the experimental samples presented in this work.

Regarding *FF*, in Figure 6(c) we can observe that both models agree well for short pitches while FF decreases faster for 1D simulations when pitch is increased. Based on this fact, this difference must be attributed to differences in modeling ohmic losses at the base. Figure 8 shows r_{base} as a function of forward voltage for S_{cont}= 2x10^3 cm/s and *p*= 200 and 800 μm extracted from 3D simulations. The corresponding values used for 1D simulations calculated with equation (5) are also shown for direct comparison. As it can be observed, under low injection conditions (V ≤ 0.5 V) r_{base} is flat for both models. For the short pitch, r_{base} values coincide while for the long pitch the value extracted from 3D simulations is lower than the one

calculated with equation (5). The boundary condition for the theoretical calculation applied in equation (5) is an equipotential surface at the opposite surface of the base contact, i.e. the emitter/base junction is forward biased to the same potential along the entire front surface [10]. From 3D simulations we can observe that this condition is no longer fulfilled as pitch increases due to the emergence of lateral current paths along the base leading to an overestimation of r_{base}. Additionally, as it is shown for 3D simulations r_{base} decreases with higher injection levels as a consequence of the reduction of the base resistivity, i.e. base conductivity modulation. Although this second effect scarcely reduces r_{base} at the the maximum power point for the simulated devices (about 0.53 V for the simulations shown in Figure 8), important deviations in *FF* could be found when low-doped substrates are used.

From V_{oc} and *FF* comparison between 1D and 3D simulations, one can conclude that with simple 1D modelling V_{oc} is overestimated while *FF* is underestimated. From the point of view of conversion efficiency, these two deviations compensate each other and the maximum achievable efficiency is approximately the same. However, among these two effects, the most important is the *FF* deviation where 1D simulations yield higher r_{base} values and, thus, shorter optimum pitch values are found.

4. Conclusions

In this work, we present a 3D model for rear locally contacted c-Si solar cells on 2.2 Ωcm p-type substrates. This model is validated using fabricated devices for different pitches allowing us to detect technological issues in our fabrication process. Additionally, 3D simulations are compared to simpler and widely-used 1D approach. Large deviations for 1D modeling in V_{oc} are determined related to strongly distorted Δn profiles due to the simplification to an unique $S_{eff\text{-}rear}$ value of the rear recombination processes. 1D models tend to overestimate V_{oc} for

devices with poorly passivated contacts and relatively low-doped substrates. Moreover, base resistivity losses are overestimated by the 1D analytical model leading to lower *FF* values and shorter optimum pitch values. From these results we can conclude that 3D simulations are mandatory for a correct modeling of V_{oc} and *FF* and then optimization of the rear contact pattern.

References

[1] Fisher M, Metz A, Raithel S. SEMI International Technology Roadmap for Photovoltaics (ITRPV) – Challenges in c-Si Technology for Suppliers and Manufacturers. *Proceedings of the 27th European Photovoltaic Conference*, 2012; 527-532.

[2] Glunz SW. High-efficiency crystalline silicon solar cells. *Advances in OptoElectronics* 2007; **2007**: 1-15.

[3] Blakers AW, Wang A, Milne AM, Zhao J, Green MA. 22.8% Efficient Silicon Solar Cell. Appl. Phys. Lett. 1989; **55**: 1363-1365.

[4] Schneiderlöchner E, Preu R, Lüdemann R, Glunz SW. Laser-fired rear contacts for crystalline silicon solar cells. *Progress in Photovoltaics: Research and Applications* 2002; **10**: 29-34.

[5] Glunz, SW, Schneiderlöchner E, Kray D, Grohe A, Hermle M, Kampwerth H, Preu R, Willeke G. Laser-fired contact silicon solar cells on p- and n-substrates. *Proceedings of the 19th European Photovoltaic Conference* 2004; 408-411.

[6] Martín I, Ortega P, Colina M, Orpella A, López G, Alcubilla R. Laser processing of Al_2O_3/a-SiC_x:H stacks: a feasible solution for the rear surface of high-efficiency p-type c-Si solar cells. *Progress in Photovoltaics: Research and Applications* 2012; DOI: 10.1002/pip.2207.

[7] Fischer B. Loss Analysis of Crystalline Silicon Cells using Photoconductance and Quantum Efficiency Measurements. Ph.D. Thesis, University of Konstanz. Cuvillier: Göttingen, 2003; Chapter 2.3.

[8] Wolf A, Biro D, Nekarda J, Stumpp S, Kimmerle A, Mack S, Preu R. Comprehensive analytical model for locally contacted rear surface pasivated solar cells", *J. Appl. Phys.* 2010; **108**: 124510.

[9] Saint-Cast P, Rüdiger M, Wolf A, Hofmann M, Rentsch J, Preu R. Advanced analytical model for the effective recombination velocity of locally contacted surfaces. *J. Appl. Phys.* 2010*;* **108**: 013705.

[10] Plagwitz H, Brendel R. Analytical model for the diode saturation current of point-contacted solar cells. *Progress in Photovoltaics: Research and Applications* 2006; **14**: 1-12.

[11] Ortega P, Orpella A, López G, Martín I, Voz C, Alcubilla R, Sánchez-Aniorte I, Colina M, Perales F, Molpeceres C. Optimization of the rear point contact scheme of crystalline silicon solar cells using laser-fired contacts. *Proceedings of the 25th European Photovoltaic Conference* 2010; 2126-2129.

[12] Cuevas A. Geometrical analysis of solar cells with partial rear contacts. *IEEE journal of Photovoltaics* 2012; **2**: 485-493.

[13] Aberle AG, Heiser G, Green MA. Two dimensional numerical optimization study of the rear contact geometry of high efficiency silicon solar cells. *J. Appl. Phys.* 1994; **75**: 5391–5405.

[14] Kotsovos K, Misiakos K. Three-dimensional simulation of carrier transport effects in the base of rear point contact silicon solae cells. *J. Appl. Phys.* 2001; **91**: 2491-2496.

[15] Renshaw J, Kang MH, Meemongkolkiat V, Rohatgi A, Carlson D, Bennett M. 3D-modeling of a back point contact solar cell structure with a selective emitter. *Proceedings of. 34th IEEE Photovoltaic Specialists Conference PVSC* 2009; 000375-000379.

[16] Zanuccoli M, De Rose R, Magnone P, Sangiorgi E, Fiegna C. Performance analysis of rear point contact solar cells by three-dimensional numerical simulation. *IEEE trans. Electron Devices* 2012; **59**: 1311-1319.

[17] Altermatt P. Models for numerical device simulations of crystalline silicon solar cells-a review. *Journal of Computational Electronics* 2011; **10**: 314–330.

[18] López-González JM, and Schröter M. Study of emitter width effects on B_f, f_t, and f_{max} of 200 GHZ SiGe HBTs by DD, HD, and EB device simulation. *Semiconductor Science and Technology* 2009; **24**: 115005.

[19] ATLAS http://www.silvaco.com/products/device_simulation/atlas.html

[20] Ortega P, Martín I, López G, Colina M, Orpella A, Voz C, Alcubilla R. p-type c-Si solar cells based on rear side laser processing of Al_2O_3/a-SiC$_x$:H stacks. *Solar Energy Materials and Solar Cells* 2012; **106**: 80-83.

[21] Clugston DA, Basore PA. PC1D version 5:32-bit solar cell modeling on personal computers. *Proceedings of the 26th IEEE Photovoltaic Specialists Conference*, pp. 207-210, 1997.

[22] Slotboom JW, De Graaf HC. Measurements of Bandgap Narrowing in Silicon Bipolar Transistors. *Solid State Electronics* 1976; **19**: 857-862.

[23] Caughey DM, Thomas RE. Carrier Mobilities in Silicon Empirically Related to Doping and Field. *Proceedings of the IEEE* 1967; **55**: 2192-2193.

Tables

Table I. S_{cont} and $r_{c\text{-}rear}$ values determined by the best fit of the experimental values.

	S_{cont}	$r_{c\text{-}rear}$
	(cm/s)	(mΩcm^2)
1 hour	3.5×10^4	2
1 day	8×10^3	10

Table II. Calculations of ΔV_{Dember} and $\Delta V_{electrochemical}$ from 3D simulations carrier profiles at open circuit conditions. The total potential drop by these two effects ΔV_{total} is also shown in the table and accounts for the difference between $V_{oc\text{-}3D}$ and $V_{oc\text{-}1D}$. The last line corresponds to the same calculations for a 0.4 Ωcm p-type substrate.

ρ_B	S_{cont}	$\Delta n(x)$		ΔV_{Dember}	$\Delta V_{electrochemical}$	ΔV_{total}	$V_{oc\text{-}3D}$	$V_{oc\text{-}1D}$
		x=0	x=w					
(Ωcm)	(cm/s)	(cm^{-3})	(cm^{-3})	(mV)	(mV)	(mV)	(mV)	(mV)
2.2	5×10^{6}	1.7×10^{15}	2.3×10^{12}	8.1	6.0	14.1	652	670
2.2	3.5×10^{4}	2.0×10^{15}	5.1×10^{14}	5.8	4.9	10.7	662	674
2.2	2×10^{3}	2.6×10^{15}	2.2×10^{15}	1.1	1.2	2.3	678	681
0.4	5×10^{6}	6.2×10^{14}	1.0×10^{13}	0.4	0.4	0.8	679	680

APPENDIX A

Table III. Summary of the most relevant parameters used in the simulations

Carrier statistics	Fermi-Dirac, complete ionization of impurities
Energy gap (E_{gap})	1.12 eV @ 300 K
Badgap narrowing	Slotboom model [22] yielding $n_{i,eff} = 8.56 \times 10^9$ cm^{-3} @ 298 K
Carrier mobility	Caughey-Thomas model [23]
Bulk Recombination	
Shockley-Read-Hall	Defect level at midgap, $\tau_{n0} = \tau_{p0} = 0.5$ s
Auger	$R_{Auger} = C_{An}\left(p \cdot n^2 - n \cdot n_i^2\right) + C_{Ap}\left(n \cdot p^2 - p \cdot n_i^2\right)$
	$C_{An} = C_{An,l}\left(\dfrac{N_D}{N_D + p}\right) + \dfrac{C_{A,h}}{2}\left(\dfrac{p}{N_D + p}\right)$
	$C_{Ap} = C_{Ap,l}\left(\dfrac{N_A}{N_A + n}\right) + \dfrac{C_{A,h}}{2}\left(\dfrac{n}{N_A + n}\right)$
	with $C_{An,l} = 2.2 \times 10^{-31}$ cm^6/s, $C_{Ap,l} = 9.9 \times 10^{-32}$ cm^6/s, and $C_{A,h} = 1.66 \times 10^{-30}$ cm^6/s [21]
Radiative	$B = 4.7 \times 10^{-15}$ cm^{3}s^{-1} [17]
Surface Recombination	
Contacted areas	At the front surface, n and p are forced to equilibrium concentrations n_0 and p_0 respectively.
	At the rear contact, current flows are modeled with:
	$J_n = q\, S_n\, (n-n_0)$
	$J_p = q\, S_p\, (p-p_0)$

	Majority carrier (holes) flow is described with $S_p = 5 \times 10^6$ cm/s. Minority carrier (electrons) flow is described with $S_n = S_{cont}$ as discussed in the text.
Passivated Front surface	Defect level at midgap, $S_{n0} = S_{p0} = 1000$ cm/s
Passivated Rear surface	Defect level at midgap, $S_{n0} = S_{p0} = S_{pas} = 10$ cm/s
Doping parameters	
Bulk acceptor density, N_A	6.5×10^{15} cm^{-3} leading to $\rho_B = 2.2$ Ωcm
Emitter regions	Gaussian distribution of phosphorus atoms, surface concentration 10^{19} cm^{-3}, depth factor $\sigma\square = 0.39$ μm, and junction depth 1 μm.

Figure captions

Figure 1. (a) Basic domain for cell of pitch 300 µm; (b) 2D cross section of the device defined at the plane in grey color.

Figure 2. Standard AM1.5G $S_{AM1.5G}$ (λ) and modified spectral irradiance S_{in} (λ). S_{in} (λ) is calculated using equation (1) with the experimental solar cell reflectance $R_{exp}(\lambda)$ shown in the graph.

Figure 3. Simulated (line) and experimental (squares) Internal quantum efficiency IQE for at solar cell with pitch=650 µm.

Figure 4. Photovoltaic values for fabricated devices (squares) and simulations (crosses). It must be mentioned that the main responsible of the difference in J_{sc} observed between both series is related to a different experimental front reflectance included in the model in the way explained in section 2.2. Lines are a guide for the eye.

Figure 5. Conversion efficiency as a dependence of pitch extracted from 3D simulations for Scont =2×10^3 cm/s and 3.5×10^4 cm/s with rc-rear= 2 mΩcm^2. The optimum pitch shifts from about 550 µm to 350 µm with the reduction in S_{cont}. Lines are a guide to the eye.

Figure 6. Comparison between 1D (lines) and 3D simulations (symbols) of the photovoltaic figures as a function of rear pitch for S_{cont}= 2×10^3 and 5×10^6 cm/s. Big discrepancies can be found in V_{oc} and *FF* impacting on optimum pitch values.

Figure 7. (a) 2D plot of *Δn* along the device at a surface centered at the contacts for S_{cont}= 5×10^6 cm/s and *p*= 800 µm. (b) Direct comparison of *Δn* profile from 1D simulations to 3D simulations where *Δn* is evaluated along a line (y=400 µm) between the contacts. The simplification to a single $S_{eff\text{-}rear}$ value leads to a strongly distorted *Δn* profile for 1D simulations. *Δn* profiles are evaluated in both cases at open circuit conditions.

Figure 8. Dependence of r_{base} on forward voltage extracted from 1D analytical model (lines) and 3D simulations (symbols) for *p*= 200 and 800 µm. At low injection (*V*<0.5 V) for short pitches both models agree while a lower r_{base} is determined from 3D modeling for the long pitch. Additionally, further reduction in r_{base} is observed due to carrier injection.